REDIRECTING GLIOBLASTOMA INFILTRATION USING MECHANOTACTIC BIOMATERIALS

Claudia B. Huesa Carballo[1,2], Aroa Cernadas Pazos[3], Alejandra Ortells Aguiar[2], Alba Ferreirós[1,3], Francesco Baschieri[4], Cristóbal Fernández Santiago[2,5], Nicolás Costa Fraga[2], Rafael López-López[1,2,3,5,6], Miguel Abal[1,2,4,5] & Jorge Barbazán[2,3]

[1]University of Santiago de Compostela, Spain. [2] Translational Oncology Laboratory (Oncomet). Health Research Institute of Santiago de Compostela, Spain. [3]Batea Oncology S.L, Spain. [4]Institute of Pathophysiology. Medical University Innsbruck, Innsbruck, Austria. [5]Centro de Investigación Biomédica en Red de Cáncer (CIBERONC), Madrid, Spain. [6]Medical Oncology department, University Clinical Hospital of Santiago de Compostela, Spain.

ABSTRACT Glioblastomas (GB) are highly aggressive tumors with a strong infiltrative pattern that renders the disease nearly uncontrollable with surgery. Residual GB cells invade along topographical and mechanical cues within the tumor microenvironment, including vessels and nerves, and typically migrate toward stiffer tissue regions through durotaxis, a migration mode driven by substrate mechanosensing via focal adhesions and actomyosin contractility. In this work, we sought to therapeutically exploit this intrinsic cellular behavior to redirect GB infiltration toward a controlled location using mechanotactic biomaterials, designed to guide tumor cells into a mechanically-controlled structure, with the goal of limiting invasion into healthy brain tissue. For this, we engineered macroporous polycarbonate-polyurethane (PCPU) collagen-coated scaffolds, significantly stiffer than brain tissue (140 vs 2 kPa). Using 2D and 3D culture systems, softer porous materials as well as genetic perturbations of durotaxis-associated genes in cancer cells, we first demonstrated that durotaxis is the main driver of scaffold-infiltration. These results were then validated in orthotopic syngeneic GB in vivo models, in which we observed a 70% reduction of invasive tumor foci compared to controls. We also characterized the intra-scaffold tumor ecosystem, which is composed primarily of tumor cells (60%), along with microglia, monocyte-derived macrophages, T cells, and endothelial cells that created neo-vasculature. Finally, we showed that, in combination with radiation therapy, the implant of mechanotactic scaffolds increased the tumor ablative effects of radiation. Importantly, these effects were not observed when implanting materials matching brain stiffness, reinforcing the relevance of the material's mechanics. Altogether, our findings support the idea of taking advantage of inherent cellular biophysical properties like durotaxis as a strategy to prevent tumor invasion, introducing the concept of mechanotherapeutics as a novel tool in cancer therapy.

Scaffold Implant Limits Invasion in GB Models *In Vivo*

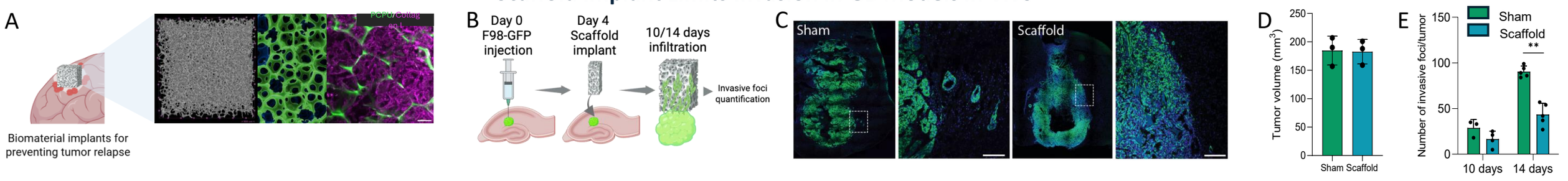

Intra-scaffold Tumor Ecosystem is composed primarily of Tumor cells, along with Microglia, Monocyte-derived Macrophages, T-cells and Others

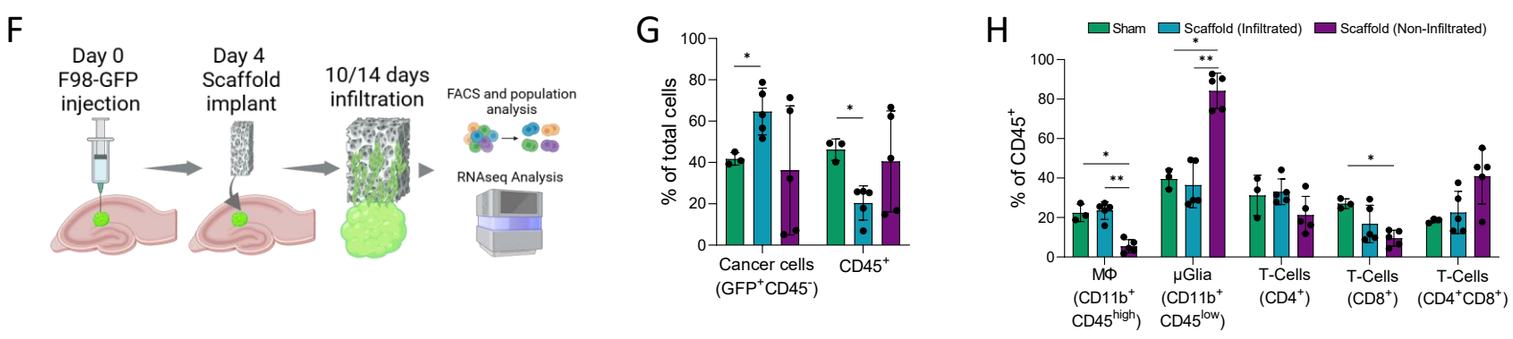

Figure 1. A) Scheme representing the strategy of implanting the biomaterial after surgery and representative scaffold structure images. From left to right: μCT; SEM; Immunofluorescence (confocal). Scale BAR: 200μm. **B)** Syngeneic GB tumor-bearing rat models stereotactically injected and then implanted with scaffolds. **C)** Reduction in brain-invasive tumor foci in implanted animals. Scale bars: 100μm. No differences were found in tumor´s volume **(D)**. Comparison between Sham and Scaffold groups at 10 days (n = 3 for Sham; n = 4 for Scaffold) and 14 days (n = 5 for both) post-device implantation **(E)**. **F)** Infiltrating tumor cells were later isolated by FACS for RNA-seq analysis. We observed a rearrangement of certain TME populations, particularly microglia and T cells, upon scaffold´s implant **(G,H)**.

Scaffold Mechanical Properties Influence Tumor Cell Infiltration

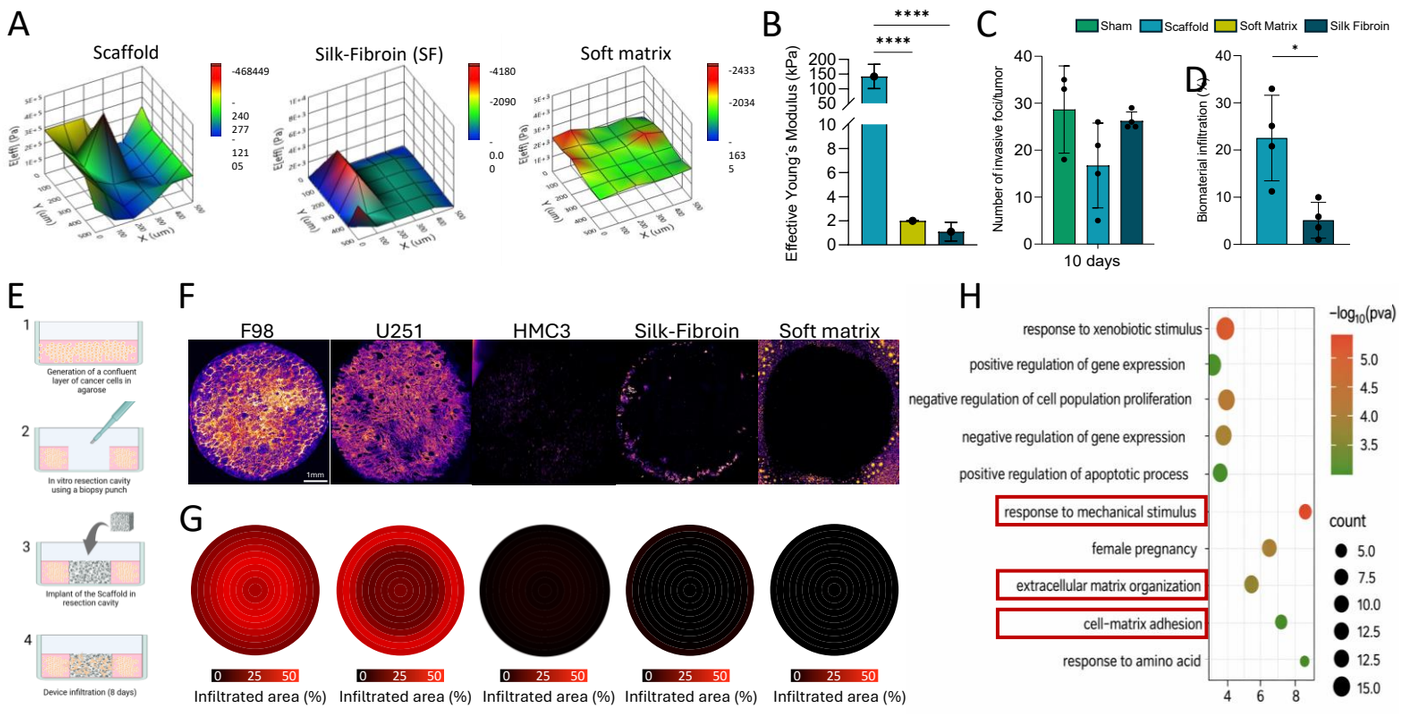

Figure 2. A) Effective Young's Modulus. color-scale adjusted. **B)** Mean ± SEM Effective Young´s Modulus of both synthetic biomaterials (n=19 for PCPU-Scaffold; n=5 for Silk Fibroin-Scaffold) and the collagen-agarose mixture (n=36). **C)** Results in vivo showing Invasive foci using soft Silk Fibroin sponges (n = 4) at 10 days post-device implantation. **D)** In vivo infiltration is reduced when using silk-fibroin scaffolds (n=4). **E)** In vitro scaffold infiltration assay setup for non-spheroid GB cell lines. **F)** Representative images of integrated density (LUT Fire) of different cell lines on different surfaces. From left to right: F98-scaffold, U251-scaffold, HMC3-scaffold, U251-silk-fibroin, U87-collagen-agarose mixture. **G)** Target plots showing the percentage of the biomaterials filled after 8 days of infiltration. From left to right: F98-scaffold (n=6), U251-scaffold (n=7), HMC3-scaffold (n=3), U251-silk fibroin (n=1), U87-soft matrix (n=1). **H)** In vitro RNA-seq gene enrichment analysis of F98 cells: scaffold-infiltrating versus sham conditions suggest changes in cellular mechanics due to scaffold infiltration.

Durotaxis drives specific colonization of scaffolds by tumor cells

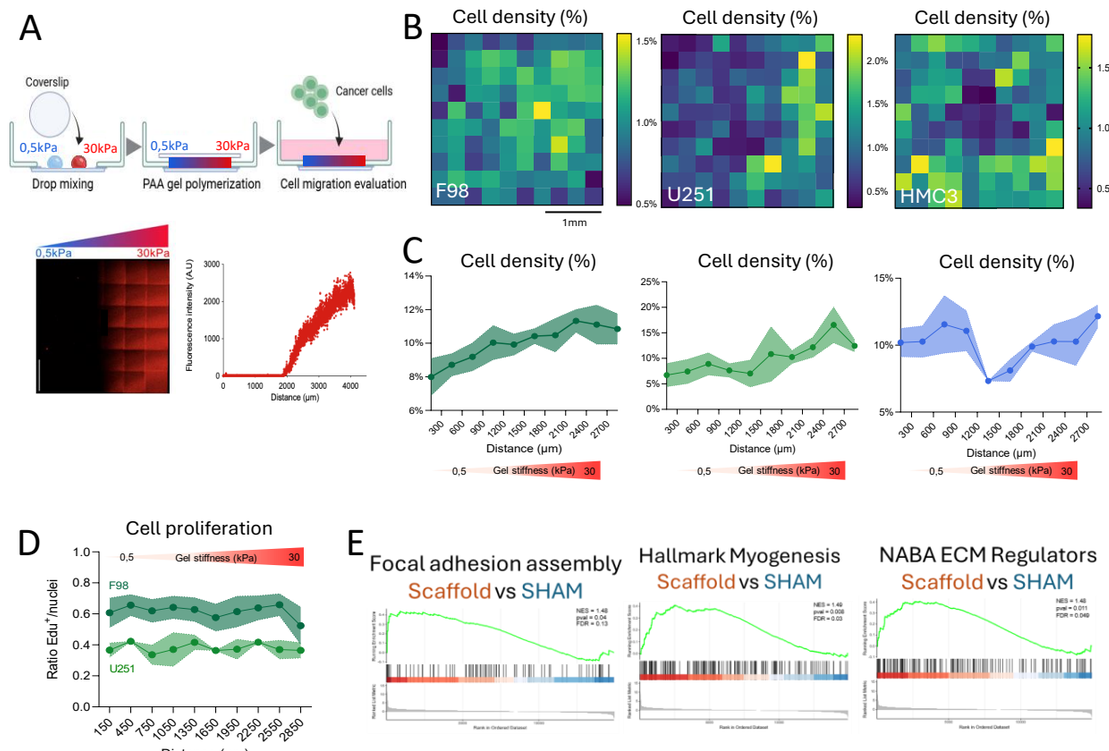

Figure 3. A) Experimental setup of a polyacrylamide gel with a stiffness gradient (0.5–30 kPa) to study durotactic-migration in GBM cell lines. **B)** Confocal microscopy at 48h showing: Cell density per 10×10 area with central gradient for F98 cells (n=6), U251 cells (n=3) and HMC3 cells (n=2). **C)** Cell density pattern of both cell lines, F98 (Top) and U251 (Bottom). **D)** % of proliferative cells measured via EdU incorpotation for F98 cells (n=6), U251 cells (n=3) and HMC3 cells (n=2). E**)** GSEA was performed for the identification of enriched sets with pval<0.05 when comparing tumor vs sham: scaffold-infiltrating cells showed upregulation of durotaxis related hallmarks. **F)** Confocal microscopy at 48h showing: Cell density per 10×10 area with central gradient for U251 shCTRL cells (n=3) and U251 TLN1 knock down cells (n=3). **G)** Levels of Talin 1 measured by qPCR of U251 cell line. **H)** Cell density pattern comparison between both cell lines. **I)** Integrated density (LUT Fire) of U251 shCTRL and shTLN1 (n=1). **J)** The infiltration assay performed with U251 shCTRL and U251 shTLN1 showed that downregulating Talin 1 reduced scaffold infiltration. Top panel: U251 shCTRL Target plot (n=6); Bottom panel: U251 shTLN1 Target plot (n=6).

Scaffold Implantation + Radiotherapy Improves Animal Survival and Reprograms The TME Toward an Antitumoral Phenotype

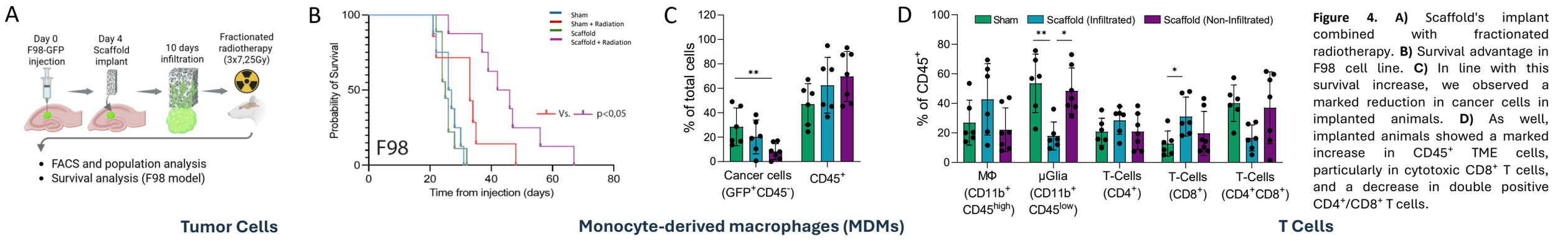

Figure 4. A) Scaffold's implant combined with fractionated radiotherapy. **B)** Survival advantage in F98 cell line. **C)** In line with this survival increase, we observed a marked reduction in cancer cells in implanted animals. **D)** As well, implanted animals showed a marked increase in $CD45^+$ TME cells, particularly in cytotoxic $CD8^+$ T cells, and a decrease in double positive $CD4^+/CD8^+$ T cells.

Tumor Cells **Monocyte-derived macrophages (MDMs)** **T Cells**

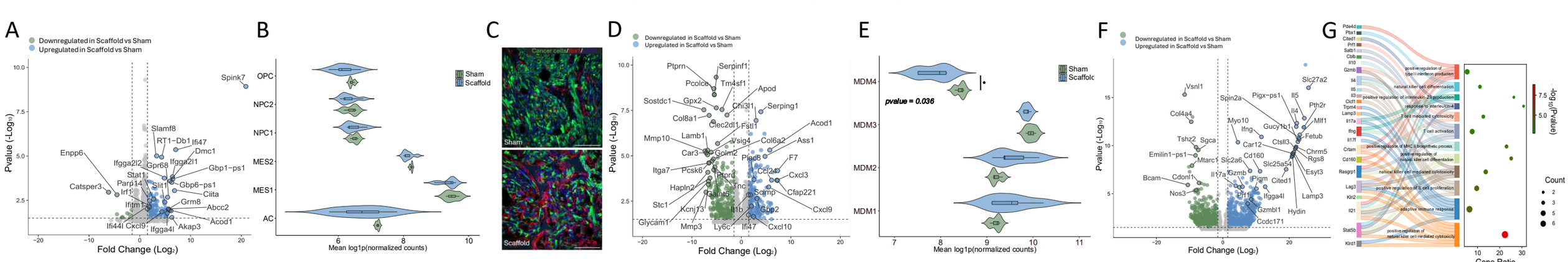

Figure 5. A) Volcano plot showing differential gene expression in tumor cells between Sham and Scaffold conditions post-radiotherapy (Filters: pvalue<0.05; FC<1.3). **B)** Signature scores across glioblastoma Kloosterman´s signature, curated from Neftel´s described states. **C)** Confocal images showing higher levels of macrophages (Iba1) in the scaffold after irradiation in comparison with sham animals. **D)** Volcano plot showing differential gene expression in Monocyte-derived macrophages population between Sham and Scaffold conditions post-radiotherapy (Filters: pvalue<0.05; FC<1.3). **E)** Signature scores across macrophage states. **F)** Volcano plot showing differential gene expression in T cell population between Sham and Scaffold conditions post-radiotherapy (Filters: pvalue<0.05; FC<1.3). **G)** Sankey Dot Plot for GO analysis (SRplot) showing principal T cell dysregulated genes and their biological functions after RT.

CONCLUSIONS

- The infiltration pattern of GB can be modulated through the implantation of scaffolds, which reduce new tumor invasion by selectively promoting a durotaxis-driven migration of tumor cells into the biomaterial.
- The scaffold primarily recapitulates the tumor fraction of the GB ecosystem, with monocyte-derived macrophages (MDMs) representing the predominant non-tumoral cell population.
- Scaffold implant, in combination with radiation therapy, improves animal survival, decreases myeloid-driven immunosupression and increases cytotoxic T cell infiltration and activation.
- **Our results indicate that a mechanotherapy-based strategy can be used to manage tumor relapse in GB, enabling tumor invasion control through mechanosensing and boost the response to conventional therapies.**

CONTACT: claudiabetsabe.huesa@rai.usc.gal

Beca Predoutoral da Universidade de Santiago de Compostela

Proyecto PID-2023-152440OA-I00 financiado por MCIU/AEI/10.13039/501100011033/FEDER,UE